International Journal of Bifurcation and Chaos, Vol. 16, No. 4 (2006) 945–959

SPATIAL RESONANCE OVERLAP IN BOSE–EINSTEIN CONDENSATES IN SUPERLATTICE POTENTIALS

VIVIEN P. CHUA
Institute for Computational Mathematics and Engineering, Stanford University, Stanford, CA 94305, USA
vchua@stanford.edu

MASON A. PORTER
Department of Physics and Center for the Physics of Information, California Institute of Technology, Pasadena, CA 91125, USA
mason@caltech.edu

Received December 17, 2004; Revised May 31, 2005

We employ Chirikov's overlap criterion to investigate interactions between subharmonic resonances of coherent structure solutions of the Gross–Pitaveskii (GP) equation governing the mean-field dynamics of cigar-shaped Bose–Einstein condensates in optical superlattices. We apply a standing wave ansatz to the GP equation to obtain a parametrically forced Duffing equation describing the BEC's spatial dynamics. We then investigate analytically the dependence of spatial resonances on the depth of the superlattice potential, deriving an order-of-magnitude estimate for the critical depth at which spatial resonances with respect to different lattice harmonics first overlap. We also derive a formula for the size of resonance zones and examine changes in our estimates as the relative superlattice amplitudes corresponding to the different harmonics are adjusted. We investigate the onset of global chaos and support our analytical work with numerical simulations.

Keywords: Bose–Einstein condensates; Hamiltonian systems; Chirikov's overlap criterion.

1. Introduction

Bose–Einstein condensation was predicted in the 1920s by Satyendra Nath Bose and Albert Einstein and was first observed experimentally in 1995 using dilute vapors of sodium and rubidium that had been cooled to temperatures near absolute zero [Anderson *et al.*, 1995; Davis *et al.*, 1995]. A magnetically-trapped gas was brought to temperatures of a few hundred nanokelvins by laser cooling, left to expand by switching off the confining trap, and subsequently imaged with optical methods. The gas was observed to reside in the lowest quantum (ground) state, creating a Bose–Einstein condensate (BEC), which consists of several thousand to several million atoms. A sharp peak in the velocity distribution observed below a critical temperature indicated that condensation had occurred [Pethick & Smith, 2002; Dalfovo *et al.*, 1999; Ketterle, 1999; Burnett *et al.*, 1999].

BECs are inhomogeneous, so they can be observed in both momentum and coordinate space [Dalfovo *et al.*, 1999]. They have two characteristic length scales: the harmonic oscillator length $a_{ho} = \sqrt{\hbar/(m\omega_{ho})}$ (which is on the order of a few microns), where $\hbar$ is Planck's constant, m is the mass of the atomic species, and $\omega_{ho} = (\omega_x\omega_y\omega_z)^{1/3}$ is the geometric mean of the trapping frequencies; and the mean healing length $\chi = 1/\sqrt{8\pi|a|\bar{n}}$,

where $\bar{n}$ is the mean density and a, the (two-body) s-wave scattering length, is determined by the atomic species of the condensate [Pethick & Smith, 2002; Dalfovo *et al.*, 1999; Köhler, 2002; Baizakov *et al.*, 2002]. When a is positive, the condensate atoms repel each other; when a is negative, the atoms attract each other; and when $a = 0$, the atoms are in the ideal gas regime. Additionally, the scattering length can be adjusted using a magnetic field in the vicinity of a Feshbach resonance [Donley *et al.*, 2001].

When considering two-body, mean-field interactions, the condensate wave function ("order parameter") $\psi(x,t)$ is described by the Gross–Pitaevskii (GP) equation. When placed in a cigar-shaped trap, BECs are modeled in the quasi-one-dimensional (quasi-1D) regime, which is valid when the transverse dimensions of the condensate are on the order of its healing length and its longitudinal dimension is much larger than its transverse ones [Bronski *et al.*, 2001a; Bronski *et al.*, 2001b; Bronski *et al.*, 2001c; Dalfovo *et al.*, 1999]. In the quasi-1D regime, one employs the 1D limit of a 3D mean-field theory rather than a true 1D mean-field theory, which would be appropriate for transverse dimensions on the order of the atomic interaction length or the atomic size [Bronski *et al.*, 2001a; Bronski *et al.*, 2001b; Bronski *et al.*, 2001c; Salasnich *et al.*, 2002; Band *et al.*, 2003]. In this situation, the GP equation has one spatial dimension and is written

$$i\hbar\psi_t = -\left[\frac{\hbar^2}{2m}\right]\psi_{xx} + g|\psi|^2\psi + V(x)\psi, \qquad (1)$$

where $|\psi|^2$ is the number density, $V(x)$ is an external potential, $g = [4\pi\hbar^2 a/m][1 + \mathcal{O}(\zeta^2)]$, and $\zeta = \sqrt{|\psi|^2|a|^3}$ is the dilute gas parameter [Dalfovo *et al.*, 1999; Köhler, 2002; Baizakov *et al.*, 2002].

Potentials $V(x)$ of interest include harmonic traps, periodic lattices, superlattices [Peil *et al.*, 2003; Rey *et al.*, 2004] and periodically (and quasiperiodically) perturbed harmonic traps. The ability to conduct experiments on quasi-1D BECs motivates the study of low-dimensional models such as (1). The case of periodic and quasiperiodic potentials without a confining trap along the dimension of the lattice or superlattice is of particular interest. Such potentials have been used, for example, to study Josephson effects [Anderson & Kasevich, 1998], squeezed states [Orzel *et al.*, 2001], Landau–Zener tunneling and Bloch oscillations [Morsch *et al.*, 2001], the transition between superfluidity and Mott insulation at both the classical [Smerzi *et al.*, 2002; Cataliotti *et al.*, 2003] and quantum [Greiner *et al.*, 2002] levels, and controllable soliton manipulation [Porter *et al.*, 2006]. Moreover, with each lattice site occupied by one alkali atom in its ground state, BECs in optical lattices show promise as registers in quantum computers [Porto *et al.*, 2003; Vollbrecht *et al.*, 2004].

In experiments, a weak harmonic trap is typically used on top of the optical lattice or superlattice to prevent the particles from escaping. (The lattice is generally turned on after the trap.) In this paper, we consider superlattice potentials of the form

$$V(x) = \varepsilon[V_1\cos(\kappa_1 x) + V_2\cos(\kappa_2 x)], \qquad (2)$$

where $\kappa_1 < \kappa_2$ without loss of generality, $V_1 = V_0\cos\theta$, and $V_2 = V_0\sin\theta$. The superlattice's primary wave number is κ_1 and its secondary wave number is κ_2. Varying θ allows one to adjust the relative contributions of the superlattice potential's associated primary and secondary harmonics. The wave numbers κ_i and superlattice amplitudes V_i are also experimentally adjustable [Peil *et al.*, 2003].

The dynamics of BECs in superlattices has recently started to garner some attention [Porter & Kevrekidis, 2005; van Noort *et al.*, 2004; Louis *et al.*, 2004; Louis *et al.*, 2005; Eksioglu *et al.*, 2004], as this system has novel, stable spatially extended states and can be used for controllable soliton manipulation. Only the case $\kappa_2 = 3\kappa_1$, has been prepared experimentally [Peil *et al.*, 2003], but superlattices with other ratios (such as $2\kappa_2 = 3\kappa_1$) can be constructed by adjusting the laser beams used to create the optical superlattice. In the present work, we consider all real ratios κ_2/κ_1. The superlattice potential (2) is quasiperiodic when κ_2/κ_1 is irrational and periodic when it is rational.

The remainder of this paper is organized as follows. In Sec. 2, we derive a parametrically forced Duffing oscillator, which describes the condensate's spatial dynamics, by applying a coherent structure ansatz to the GP equation (1). This is followed by a discussion in Sec. 3 of Chirikov's overlap criterion, which we apply to attractive BECs with both positive and negative chemical potentials to estimate the lattice height required for the onset of globally chaotic dynamics. We also derive an expression

for the size of resonance zones. In Sec. 4, we compare our analytical estimates to numerically computed Poincaré sections. We summarize our results in Sec. 5.

2. Coherent Structures

We consider uniformly propagating coherent structures with the ansatz

$$\psi(x,t) = R(x)\exp(i\,[\theta(x) - \mu t]), \tag{3}$$

where R is the amplitude of the wave function, $\theta(x)$ determines its phase, $\mathbf{v} \propto \nabla\theta$ is the particle velocity, and μ is the BEC's chemical potential. When the (temporally periodic) coherent structure (3) is also spatially periodic, it is called a *modulated amplitude wave* (MAW) [Brusch *et al.*, 2000; Brusch *et al.*, 2001]. The orbital stability of MAWs for the cubic NLS with elliptic function potentials has been studied by Bronski and co-authors [Bronski *et al.*, 2001a; Bronski *et al.*, 2001b; Bronski *et al.*, 2001c]. To obtain stability information with sinusoidal potentials, one takes the limit as the elliptic modulus k approaches zero [Lawden, 1989; Rand, 1994].

Substituting (3) into the GP equation (1) and equating real and imaginary parts yields

$$\begin{aligned}\hbar\mu R(x) = &-\frac{\hbar^2}{2m}R''(x) + \left[\frac{\hbar^2}{2m}[\theta'(x)]^2\right.\\ &\left. + gR^2(x) + V(x)\right]R(x),\\ 0 = &\frac{\hbar^2}{2m}\left[2\theta'(x)R'(x) + \theta''(x)R(x)\right].\end{aligned} \tag{4}$$

This, in turn, yields the following nonautonomous, two-dimensional system of nonlinear ordinary differential equations [Bronski *et al.*, 2001b; Porter & Cvitanović, 2004a, 2004b]:

$$\begin{aligned}R' &= P_R,\\ P_R' &= \frac{c^2}{R^3} - \frac{2m\mu R}{\hbar} + \frac{2mg}{\hbar^2}R^3 + \frac{2m}{\hbar^2}V(x)R,\end{aligned} \tag{5}$$

where $'$ denotes differentiation with respect to x and the parameter c, determined by $\theta'(x) = c/R^2$, plays the role of "angular momentum" [Bronski *et al.*, 2001b].

When $c = 0$, Eq. (3) describes a standing wave. In this situation, Eq. (5) becomes

$$\begin{aligned}R'' + \delta R + \alpha R^3 + \varepsilon R V_1\cos(\kappa_1 x)\\ + \varepsilon R V_2\cos(\kappa_2 x) = 0,\end{aligned} \tag{6}$$

where $\delta = 2m\mu/\hbar$, $\alpha = -2mg/\hbar^2$, and $\varepsilon = -(2m/\hbar^2)V_0$. We assume that the lattice depth is shallow, so that $|\varepsilon| \ll 1$.

The unperturbed Hamiltonian (corresponding to (6) with $\varepsilon = 0$) is

$$H(R, P_R) = \frac{1}{2}P_R^2 + \frac{1}{2}\delta R^2 + \frac{1}{4}\alpha R^4. \tag{7}$$

KAM theory guarantees that locally chaotic dynamics occurs near resonances for arbitrarily small $\varepsilon > 0$ [Guckenheimer & Holmes, 1983; Lichtenberg & Lieberman, 1992]. Perturbations of Hamiltonian systems that break integrability lead to increasingly large regions of chaotic dynamics in phase space as the size of the perturbation is increased. Locally chaotic configurations have small regions of phase space with trajectories that behave erratically, but such trajectories still remain within those regions. Under sufficiently large nonintegrable forcing, however, trajectories travel from one region of phase space to another, leading to global chaos [Lichtenberg & Lieberman, 1992; Rand, 1994].

In this work, we employ Chirikov's overlap criterion to estimate the value of ε at which the dynamics of (6) first becomes globally chaotic [Rand, 1994; Lichtenberg & Lieberman, 1992]. Chaotic regions in phase space are identified from fuzziness in Poincaré sections, whereas integrable trajectories are represented by continuous curves. In the context of BECs, increasing ε corresponds to increasing the depth of the wells in the optical superlattice. Fixing the other physical parameters, we examine the development of chaotic dynamics through spatial resonance overlap as the lattice depth (which can be tuned experimentally) is increased.

It is also important to keep experimental limitations in mind. We do not incorporate a weak harmonic trap in (6), assuming instead that the superlattice is present for all x. From an experimental perspective, it cannot be ignored after some finite number of lattice minima. Thus far, BECs in regular optical lattices with up to 200 wells have been created experimentally [Pedri *et al.*, 2001]. The use of infinitely many wells is a standard theoretical approximation and the resonance overlap we study pertains experimentally to a finite number of wells

away from the edges of the weak trap, for which it is permissible to ignore perturbations due to the trap.

3. Chirikov's Overlap Criterion

Chirikov's overlap criterion is used to study the transition from local to global chaos in Hamiltonian systems. The last remaining KAM surface between primary resonances is destroyed when the sum of the half-widths of the two island separatrices formed by the resonances equals the distance between the resonances. The system's Hamiltonian is used to estimate the minimal perturbation strength ε for which these separatrices begin to touch. We derive analytical approximations for the locations and sizes of the resonance zones to estimate this critical ε when the two primary resonances first overlap, leading to the onset of global chaos [Rand, 1994; Lichtenberg & Lieberman, 1992].

A Hamiltonian system has the form

$$\frac{dq_i}{dx} = \frac{\partial H}{\partial p_i}, \quad \frac{dp_i}{dx} = -\frac{\partial H}{\partial q_i}, \quad i \in \{1, \ldots, n\}, \tag{8}$$

where the Hamiltonian $H = H(q_i, p_i, x; \varepsilon)$ can be expanded in a power series in ε as follows:

$$H(q_i, p_i, x; \varepsilon) = H_0(q_i, p_i, x) + \varepsilon H_1(q_i, p_i, x) + \varepsilon^2 H_2(q_i, p_i, x) + O(\varepsilon^3). \tag{9}$$

The nonintegrable Hamiltonian of the parametrically forced Duffing equation (which is a nonlinear Mathieu equation) (6) is

$$H = \frac{1}{2}P_R^2 + \frac{1}{2}\delta R^2 + \frac{1}{4}\alpha R^4 + \varepsilon\frac{R^2}{2}V_1\cos(\kappa_1 x) + \varepsilon\frac{R^2}{2}V_2\cos(\kappa_2 x). \tag{10}$$

We set $\varepsilon = 0$ to consider the unforced (integrable) system,

$$R'' + \delta R + \alpha R^3 = 0, \tag{11}$$

which we solve approximately by keeping a single harmonic,

$$\begin{aligned} R &= A\cos(\omega x), \\ P_R &= R' = -A\omega\sin(\omega x). \end{aligned} \tag{12}$$

One can alternatively solve (11) exactly using elliptic functions, as has been done previously for applications of Chirikov's overlap criterion to nonlinear Mathieu equations [Zounes & Rand, 2001, 2002a, 2002b]. We substitute (12) into (11) and neglect all harmonics beyond $\{\cos(\omega x), \sin(\omega x)\}$ to obtain an approximate expression for ω as a function of A,

$$\omega = \sqrt{\delta + \frac{3}{4}\alpha A^2}\,. \tag{13}$$

The next step is to transform to approximate action-angle variables. Suppose the angle is given by $q = \omega x$, so that

$$R = A\cos q, \quad q' = \omega = \sqrt{\delta + \frac{3}{4}\alpha A^2}. \tag{14}$$

The action variable p is then defined so that

$$q' = \frac{\partial H_0}{\partial p} = \frac{\partial H_0}{\partial A}\frac{\partial A}{\partial p} = \sqrt{\delta + \frac{3}{4}\alpha A^2}, \tag{15}$$

where $\partial H_0/\partial A = \delta A + (9/8)\alpha A^3$. This yields the differential equation,

$$\frac{\partial p}{\partial A} = \frac{\delta A + \frac{9}{8}\alpha A^3}{\sqrt{\delta + \frac{3}{4}\alpha A^2}}, \tag{16}$$

governing the dependence of p on A.

We substitute (12) into (10) and neglect higher harmonics to obtain

$$H = \frac{1}{2}\delta A^2 + \frac{9}{32}\alpha A^4 + \varepsilon\frac{A^2}{2}\cos^2 q[V_1\cos(\kappa_1 x) + V_2\cos(\kappa_2 x)]. \tag{17}$$

We consider attractive ($a < 0$) condensates with both positive ($\mu > 0$) and negative ($\mu < 0$) chemical potentials, although only the derivation for the latter case is presented explicitly in this paper. The same method works for attractive BECs with positive chemical potentials [Zounes & Rand, 2001, 2002a].

For negative chemical potentials, the parameters are rescaled so that $\alpha = 1$ and $\delta = -1$, which we substitute into (16) and (17) to obtain

$$\frac{\partial p}{\partial A} = \frac{-A + \frac{9}{8}A^3}{\sqrt{-1 + \frac{3}{4}A^2}} \tag{18}$$

and

$$H = -\frac{1}{2}A^2 + \frac{9}{32}A^4 + \varepsilon\frac{A^2}{2}\cos^2 q[V_1\cos(\kappa_1 x) + V_2\cos(\kappa_2 x)]\,. \tag{19}$$

We integrate (18) to yield

$$p = \frac{1}{4}A^2\sqrt{-4 + 3A^2}\,, \tag{20}$$

which implies that

$$A = \frac{1}{3}\sqrt{2d^{1/3} + 8d^{-1/3} + 4}\,, \tag{21}$$

where $d = 8 + 243p^2 + 9p\sqrt{48 + 729p^2}$.

This gives an approximate canonical transformation from $(R, P_R) \to (q, p)$:

$$\begin{aligned} R &= \frac{1}{3}\sqrt{2d^{1/3} + 8d^{-1/3} + 4}\cos q, \\ P_R &= -\frac{\omega}{3}\sqrt{2d^{1/3} + 8d^{-1/3} + 4}\sin q. \end{aligned} \tag{22}$$

The Hamiltonian (10) is thus written

$$\begin{aligned} H = {} & \frac{1}{72}[d^{1/3} + 4d^{-1/3} + 2]^2 \\ & - \frac{1}{9}[d^{1/3} + 4d^{-1/3} + 2] \\ & + \frac{\varepsilon}{9}[d^{1/3} + 4d^{-1/3} + 2] \\ & \times \cos^2 q[V_1 \cos(\kappa_1 x) + V_2 \cos(\kappa_2 x)]. \end{aligned} \tag{23}$$

3.1. *Near-identity transformations*

In this section, we apply a near-identity transformation to the nonautonomous Hamiltonian (23). This transformation has the general form [Rand, 1994; Guckenheimer & Holmes, 1983]

$$\begin{aligned} q_i &= Q_i + \varepsilon\Theta_i^{(1)}(Q_j, P_j) + \varepsilon^2\Theta_i^{(2)}(Q_j, P_j) + O(\varepsilon^3), \\ p_i &= P_i + \varepsilon\Phi_i^{(1)}(Q_j, P_j) + \varepsilon^2\Phi_i^{(2)}(Q_j, P_j) + O(\varepsilon^3), \end{aligned} \tag{24}$$

where $\Theta_i^{(k)}$ and $\Phi_i^{(k)}$ are chosen so that the transformation is canonical.

First, we extend phase space, so that (23) is written

$$\begin{aligned} \tilde{H} &= H + p_2 \\ &= \frac{1}{72}[d_1^{1/3} + 4d_1^{-1/3} + 2]^2 \\ &\quad - \frac{1}{9}[d_1^{1/3} + 4d_1^{-1/3} + 2] \\ &\quad + \frac{\varepsilon}{9}[d_1^{1/3} + 4d_1^{-1/3} + 2] \\ &\quad \times \cos^2 q_1[V_1 \cos(\kappa_1 q_2) + V_2 \cos(\kappa_2 q_2)] + p_2 \\ &\equiv \tilde{H}_0 + \varepsilon\tilde{H}_1, \end{aligned} \tag{25}$$

where $d_1 = 8 + 243p_1^2 + 9p_1\sqrt{48 + 729p_1^2}$, $p_1 = p$, $q_1 = q$, and $q_2 = x$. (The variable p_2 is the conjugate momentum of q_2.) The $O(1)$ and $O(\varepsilon)$ terms in the transformed Hamiltonian are then

$$\begin{aligned} \tilde{H}_0(q_i, p_i) = {} & \frac{1}{72}[d_1^{1/3} + 4d_1^{-1/3} + 2]^2 \\ & - \frac{1}{9}[d_1^{1/3} + 4d_1^{-1/3} + 2] + p_2, \\ \tilde{H}_1(q_i, p_i) = {} & \frac{1}{9}[d_1^{1/3} + 4d_1^{-1/3} + 2] \\ & \times \cos^2 q_1[V_1 \cos(\kappa_1 q_2) + V_2 \cos(\kappa_2 q_2)]. \end{aligned}$$

We use trigonometric identities to isolate harmonics and obtain

$$\begin{aligned} \tilde{H}_1(q_i, p_i) = {} & \frac{1}{36}[d_1^{1/3} + 4d_1^{-1/3} + 2] \\ & \times \{V_1[\cos(2q_1 + \kappa_1 q_2) \\ & + \cos(2q_1 - \kappa_1 q_2) + 2\cos(\kappa_1 q_2)] \\ & + V_2[\cos(2q_1 + \kappa_2 q_2) + \cos(2q_1 \\ & - \kappa_2 q_2) + 2\cos(\kappa_2 q_2)]\}. \end{aligned} \tag{26}$$

We define another near-identity transformation, from $(q_i, p_i) \to (Q_i, P_i)$ as

$$\begin{aligned} q_i &= Q_i + \varepsilon\frac{\partial W_1}{\partial P_i} + O(\varepsilon^2), \\ p_i &= P_i - \varepsilon\frac{\partial W_1}{\partial Q_i} + O(\varepsilon^2). \end{aligned} \tag{27}$$

We choose a generating function W_1 to simplify the transformed Hamiltonian, $K = K_0 + \varepsilon K_1 + O(\varepsilon^2)$, given by

$$\begin{aligned} K_0 &= \tilde{H}_0(Q_i, P_i) \\ &= \frac{1}{72}[D_1^{1/3} + 4D_1^{-1/3} + 2]^2 \\ &\quad - \frac{1}{9}[D_1^{1/3} + 4D_1^{-1/3} + 2] + P_2, \\ K_1 &= \tilde{H}_1(Q_i, P_i) + \{\tilde{H}_0, W_1\} \\ &= \frac{1}{36}[D_1^{1/3} + 4D_1^{-1/3} + 2] \\ &\quad \times \{V_1[\cos(2Q_1 + \kappa_1 Q_2) + \cos(2Q_1 - \kappa_1 Q_2) \\ &\quad + 2\cos(\kappa_1 Q_2)] + V_2[\cos(2Q_1 + \kappa_2 Q_2) \\ &\quad + \cos(2Q_1 - \kappa_2 Q_2) + 2\cos(\kappa_2 Q_2)]\} \\ &\quad - h\frac{\partial W_1}{\partial Q_1} - \frac{\partial W_1}{\partial Q_2}, \end{aligned} \tag{28}$$

where $D_1 = 8 + 243P_1^2 + 9P_1\sqrt{48 + 729P_1^2}$, $h = (M/108)[D_1^{1/3} + 4D_1^{-1/3} + 2][D_1^{-2/3} - 4D_1^{-4/3}] - (M/27)[D_1^{-2/3} + 4D_1^{-4/3}]$, $M = 486P_1 + 9\sqrt{48 + 729P_1^2} + 6561P_1^2/\sqrt{48 + 729P_1^2}$, and $\{H_0, W_1\}$ is the Poisson bracket of H_0 and W_1 [Rand, 1994; Goldstein, 1980].

The appropriate generating function has the form

$$W_1 = C_+^1 \sin(2Q_1 + \kappa_1 Q_2) + C_-^1 \sin(2Q_1 - \kappa_1 Q_2) + C_+^2 \sin(2Q_1 + \kappa_2 Q_2) + C_-^2 \sin(2Q_1 - \kappa_2 Q_2) + 2C_3 \sin(\kappa_1 Q_2) + 2C_4 \sin(\kappa_2 Q_2). \quad (29)$$

We choose W_1 so that the Poisson bracket $\{\tilde{H}_0, W_1\}$ eliminates all the trigonometric terms in K_1 except for a single term, a so-called "nonremovable" term pertaining to the resonance zone of interest. There are four possible choices for this term, which have corresponding prefactors C_+^i and C_-^i for $i \in \{1, 2\}$. One chooses $i = 1$ to examine resonances with respect to the primary lattice harmonic and $i = 2$ for resonances with respect to the secondary harmonic.

The coefficients C_+^1, C_-^1, C_+^2, C_-^2, C_3, and C_4 are given by the formulas

$$\begin{aligned} C_+^i &= \frac{[D_1^{1/3} + 4D_1^{-1/3} + 2]V_i}{36(2h + \kappa_i)}, \\ C_-^i &= \frac{[D_1^{1/3} + 4D_1^{-1/3} + 2]V_i}{36(2h - \kappa_i)}, \quad i \in \{1, 2\}, \\ C_3 &= \frac{[D_1^{1/3} + 4D_1^{-1/3} + 2]V_1}{36}, \\ C_4 &= \frac{[D_1^{1/3} + 4D_1^{-1/3} + 2]V_2}{36}. \end{aligned} \quad (30)$$

The denominators in C_+^i and C_-^i vanish, respectively, when $2h + \kappa_i = 0$ and $2h - \kappa_i = 0$, indicating the presence of resonance zones. In the calculation below, we consider resonances with respect to lattice harmonics due to the latter condition. We find the locations and sizes of these resonance zones and use Chirikov's overlap criterion to estimate the value of ε at which globally chaotic dynamics occurs.

We obtain [Rand, 1994]

$$K_1^{(i)} = \frac{V_i}{36}[D_1^{1/3} + 4D_1^{-1/3} + 2] \times [\cos(2Q_1 - \kappa_i Q_2)], \quad i \in \{1, 2\}, \quad (31)$$

which yields the transformed Hamiltonian

$$K^{(i)} = \frac{1}{72}[D_1^{1/3} + 4D_1^{-1/3} + 2]^2 - \frac{1}{9}[D_1^{1/3} + 4D_1^{-1/3} + 2] + P_2 + \varepsilon \frac{V_i}{36}[D_1^{1/3} + 4D_1^{-1/3} + 2] \times [\cos(2Q_1 - \kappa_i Q_2)] + O(\varepsilon^2). \quad (32)$$

3.2. *Analytical estimate of the critical lattice height*

We obtain an autonomous, one degree-of-freedom system (for a given $i \in \{1, 2\}$) with a linear, canonical transformation,

$$X_1 = 2Q_1 - \kappa_i Q_2, \quad X_2 = Q_2$$
$$Y_1 = P_1, \quad Y_2 = P_2 + \kappa_i P_1.$$

The resulting Hamiltonian is

$$K^{(i)} = \frac{1}{72}[G_1^{1/3} + 4G_1^{-1/3} + 2]^2 - \frac{1}{9}[G_1^{1/3} + 4G_1^{-1/3} + 2] + Y_2 - \kappa_i Y_1 + \varepsilon \frac{V_i}{36}[G_1^{1/3} + 4G_1^{-1/3} + 2] \cos X_1 + O(\varepsilon^2), \quad (33)$$

where $G_1 = 8 + 243Y_1^2 + 9Y_1\sqrt{48 + 729Y_1^2}$.

After the transformation, X_2 is no longer explicitly present in $K^{(i)}$ so both Y_2 and $K^{(i)}$ are constant of motions [Rand, 1994]. Therefore,

$$\begin{aligned} K^{*(i)} &= K^{(i)} - Y_2 \\ &= \frac{1}{72}[G_1^{1/3} + 4G_1^{-1/3} + 2]^2 - \frac{1}{9}[G_1^{1/3} + 4G_1^{-1/3} + 2] - \kappa_i Y_1 + \varepsilon \frac{V_i}{36}[G_1^{1/3} + 4G_1^{-1/3} + 2] \cos(X_1) + O(\varepsilon^2) \\ &= \text{constant}. \end{aligned} \quad (34)$$

We determine the equilibria from Hamilton's equations,

$$\begin{aligned} Y_1' &= -\frac{\partial K^{*(i)}}{\partial X_1} = \varepsilon \frac{V_i}{36}[G_1^{1/3} + 4G_1^{-1/3} + 2] \sin X_1, \\ X_1' &= \frac{\partial K^{*(i)}}{\partial Y_1} \\ &= \frac{N}{108}(G_1^{1/3} + 4G_1^{-1/3} + 2)(G_1^{-2/3} - 4G_1^{-4/3}) - \frac{N}{27}(G_1^{-2/3} - 4G_1^{-4/3}) - \kappa_i + \varepsilon V_i \frac{N}{108}(G_1^{-2/3} - 4G_1^{-1/3}) \cos(X_1), \end{aligned} \quad (35)$$

where $N = 486Y_1 + 9(96Y_1 + 2916Y_1^3)/(2Y_1\sqrt{48 + 729Y_1^2})$.

The condition $Y_1' = 0$ implies that equilibria (X_1^*, Y_1^*) satisfy $\sin X_1^* = 0$, so that $X_1^* = 0$ or $X_1^* = \pi$. Substituting these values into (35) for $X_1' = 0$ gives Y_1^*. For small ε, both values of X_1^* give

$$Y^{*(i)} \approx -0.843 + 2.161\kappa_i + O(\varepsilon), \tag{36}$$

where we have employed a power series expansion to approximate the value of $Y^{*(i)}$. The integrable Hamiltonian (34) has a pendulum-like separatrix. We denote the location of its saddles by $Y_s^{(i)}$ and its maximum height by $Y_m^{(i)}$. One obtains $Y_s^{(i)}$ when $X_1 = \pi$, and $Y_m^{(i)}$ occurs at the same angle ($X_1 = 0$) as the center point of (35) and has the same Hamiltonian value as the saddles (because it too lies on the separatrix). Therefore,

$$\begin{aligned} &K^*(X_1^* = 0, Y_1 = Y_m^{(i)}) \\ &\quad = K^*(X_1^* = \pi, Y_1 = Y_s^{(i)}), \quad i \in \{1, 2\}. \end{aligned} \tag{37}$$

This gives the equation

$$\begin{aligned} &\frac{1}{72}[{G_m^{(i)}}^{1/3} + 4{G_m^{(i)}}^{-1/3} + 2]^2 \\ &\qquad - \frac{1}{9}[{G_m^{(i)}}^{1/3} + 4{G_m^{(i)}}^{-1/3} + 2] - \kappa_i Y_m^{(i)} \\ &\qquad + \varepsilon\frac{V_i}{36}[{G_m^{(i)}}^{1/3} + 4{G_m^{(i)}}^{-1/3} + 2] \\ &\quad = \frac{1}{72}[{G_s^{(i)}}^{1/3} + 4{G_s^{(i)}}^{-1/3} + 2]^2 \\ &\qquad - \frac{1}{9}[{G_s^{(i)}}^{1/3} + 4{G_s^{(i)}}^{-1/3} + 2] - \kappa_i Y_s^{(i)} \\ &\qquad - \varepsilon\frac{V_i}{36}[{G_s^{(i)}}^{1/3} + 4{G_s^{(i)}}^{-1/3} + 2], \end{aligned} \tag{38}$$

where $G_m^{(i)} = 8 + 243{Y_m^{(i)}}^2 + 9Y_m^{(i)}\sqrt{48 + 729{Y_m^{(i)}}^2}$, $G_s^{(i)} = 8 + 243{Y_s^{(i)}}^2 + 9Y_s^{(i)}\sqrt{48 + 729{Y_s^{(i)}}^2}$, $Y_m^{(i)} = Y_s^{(i)} + \delta_i$ is to be determined, and $Y_s^{(i)} \approx -0.843 + 2.161\kappa_i$ is known.

We set $\delta_i = k_i\sqrt{\varepsilon} + O(\varepsilon)$ and write Eq. (38) in the form

$$\begin{aligned} &F(Y_s^{(i)} + k_i\sqrt{\varepsilon}) + \varepsilon B(Y_s^{(i)} + k_i\sqrt{\varepsilon}) \\ &\quad = F(Y_s^{(i)}) - \varepsilon B(Y_s^{(i)}), \end{aligned} \tag{39}$$

where $F(Y_s^{(i)}) = (1/72)[{G_s^{(i)}}^{1/3} + 4{G_s^{(i)}}^{-1/3} + 2]^2 - (1/9)({G_s^{(i)}}^{1/3} + 4{G_s^{(i)}}^{-1/3} + 2) - \kappa_i Y_s^{(i)}$ and $B(Y_s^{(i)}) = (V_i/36)[{G_s^{(i)}}^{1/3} + 4{G_s^{(i)}}^{-1/3} + 2]$.

We expand (39) in a power series in $\sqrt{\varepsilon}$ using $F(Y_s^{(i)} + k_i\sqrt{\varepsilon}) = F(Y_s^{(i)}) + \sqrt{\varepsilon}F'(Y_s^{(i)})k_i + (1/2)\varepsilon F''(Y_s^{(i)})k_i^2 + O(\varepsilon^{3/2})$ to obtain

$$\begin{aligned} &F(Y_s^{(i)}) + \sqrt{\varepsilon}F'(Y_s^{(i)})k_i + \frac{1}{2}\varepsilon F''(Y_s^{(i)})k_i^2 \\ &\qquad + \varepsilon B(Y_s^{(i)}) + O(\varepsilon^{3/2}) = F(Y_s^{(i)}) - \varepsilon B(Y_s^{(i)}). \end{aligned} \tag{40}$$

At $O(\sqrt{\varepsilon})$, we see that $F'(Y_s^{(i)}) = 0$. At $O(\varepsilon)$, we obtain

$$k_i = 2\sqrt{-\frac{B(Y_s^{(i)})}{\dfrac{\partial^2 F}{\partial {Y_s^{(i)}}^2}}}, \quad i \in \{1, 2\}. \tag{41}$$

Recall that $\kappa_2 > \kappa_1$. As ε is increased, individual resonance regions associated with each of the lattice harmonics begin to overlap when the minimum of the separatrix height $Y_m^{(2)}$ for the κ_2 resonance band equals the maximum of the separatrix height $Y_m^{(1)}$ of the κ_1 resonance band. Equation (41) also gives an estimate for the separatrix size, which is

$$W_i = 2\delta_i = 2k_i\sqrt{\varepsilon} + O(\varepsilon). \tag{42}$$

Resonance overlap occurs when

$$\begin{aligned} &-0.843 + 2.161\kappa_2 - k_2\sqrt{\varepsilon} \\ &\quad = -0.843 + 2.161\kappa_1 + k_1\sqrt{\varepsilon}, \end{aligned} \tag{43}$$

which yields the order-of-magnitude estimate

$$\varepsilon_{\rm cr} \approx [2.161]^2\left(\frac{\kappa_2 - \kappa_1}{k_1 + k_2}\right)^2 \approx 4.670\left(\frac{\kappa_2 - \kappa_1}{k_1 + k_2}\right)^2 \tag{44}$$

for the critical lattice height at which the transition from local to global chaos occurs. We similarly obtain an equation to estimate the critical ε for $\alpha = 1$ and $\delta = 1$ with the same analytical procedure:

$$\begin{aligned} &-3.908 + 3.430\kappa_2 - k_2\sqrt{\varepsilon} \\ &\quad = -3.908 + 3.430\kappa_1 + k_1\sqrt{\varepsilon}. \end{aligned} \tag{45}$$

While our analysis is only guaranteed to give an order-of-magnitude estimate for $\varepsilon_{\rm cr}$, our numerical simulations (discussed in the next section) reveal that this estimate can sometimes perform far better in practice. By construction, estimates obtained using Chirikov's overlap criterion give an upper bound for $\varepsilon_{\rm cr}$ because one is examining the overlap of resonance bands when all pertinent KAM tori have been destroyed [Lichtenberg & Lieberman, 1992; Rand, 1994]. Strictly speaking, the series approximation (36)

removes this guarantee, but one still nearly always obtains upper bounds in practice. (In particular, our estimate provided an upper bound for every example we studied.)

4. Numerical Simulations

To support our analytical work, we numerically simulated Eq. (6) for several values of $V_1 = V_0 \cos(\theta)$ and $V_2 = V_0 \sin(\theta)$. We examined situations with different relative contributions of the two lattice harmonics. Specifically, we considered $\theta = n\pi/16$ for $n \in \{1, \ldots, 7\}$. (When $\theta = 0$ and $\theta = \pi/2$, one of the forcing terms is identically zero, so only one resonance is being excited.) In our simulations, we scaled (6) so that $V_0 = 1$.

We tabulate our analytical and numerical estimates for $\alpha = 1$, $\delta = -1$ in Tables 1–3 and for $\alpha = 1$, $\delta = 1$ in Tables 4–6. The critical lattice depths

Table 1. Critical lattice depths for the onset of globally chaotic dynamics for a quasi-1D BEC in a superlattice with integer wave number ratio. Adjustments in θ indicate different relative contributions of the lattice harmonics. In this table, we consider attractive condensates with negative chemical potentials. The parameters are $\alpha = 1$, $\delta = -1$, and $\kappa_2 = 3\kappa_1 = 3$. As discussed in the text, the analytical results give a rough upper bound for the numerical estimates. Note additionally that V_0 (and hence V_1 and V_2) can be scaled so that $\varepsilon_{\rm cr}$ is small enough for the perturbative analysis to be valid.

θ	V_1	V_2	Analytical ε	Numerical ε
$\pi/16$	0.981	0.195	1.181	0.754
$\pi/8$	0.924	0.383	0.819	0.686
$3\pi/16$	0.831	0.556	0.667	0.521
$\pi/4$	0.707	0.707	0.592	0.422
$5\pi/16$	0.556	0.831	0.558	0.413
$3\pi/8$	0.383	0.924	0.559	0.414
$7\pi/16$	0.195	0.981	0.597	0.429

Table 2. Same as Table 1, except the superlattice has a rational wave number ratio. The parameters are $\alpha = 1$, $\delta = -1$, and $\kappa_2 = 3\kappa_1/2 = 3$.

θ	V_1	V_2	Analytical ε	Numerical ε
$\pi/16$	0.981	0.195	0.149	0.143
$\pi/8$	0.924	0.383	0.116	0.106
$3\pi/16$	0.831	0.556	0.102	0.099
$\pi/4$	0.707	0.707	0.095	0.085
$5\pi/16$	0.556	0.831	0.095	0.087
$3\pi/8$	0.383	0.924	0.101	0.089
$7\pi/16$	0.195	0.981	0.117	0.104

Table 3. Same as Table 1, except the superlattice has an irrational wave number ratio. The parameters are $\alpha = 1$, $\delta = -1$, and $\kappa_2 = \sqrt{2}\kappa_1 = \sqrt{2}$.

θ	V_1	V_2	Analytical ε	Numerical ε
$\pi/16$	0.981	0.195	0.089	0.054
$\pi/8$	0.924	0.383	0.068	0.031
$3\pi/16$	0.831	0.556	0.060	0.028
$\pi/4$	0.707	0.707	0.056	0.025
$5\pi/16$	0.556	0.831	0.056	0.026
$3\pi/8$	0.383	0.924	0.059	0.026
$7\pi/16$	0.195	0.981	0.069	0.032

Table 4. Same as Table 1, except for an attractive condensate with a positive chemical potential. The parameters are $\alpha = 1$, $\delta = 1$, and $\kappa_2 = 3\kappa_1 = 3$. Recall that V_0 (and hence V_1 and V_2) can be scaled so that $\varepsilon_{\rm cr}$ is small enough for the perturbative analysis to be valid.

θ	V_1	V_2	Analytical ε	Numerical ε
$\pi/16$	0.981	0.195	3.105	1.508
$\pi/8$	0.924	0.383	2.456	1.221
$3\pi/16$	0.831	0.556	2.245	1.043
$\pi/4$	0.707	0.707	1.657	0.882
$5\pi/16$	0.556	0.831	1.782	0.893
$3\pi/8$	0.383	0.924	2.237	1.187
$7\pi/16$	0.195	0.981	2.452	1.254

Table 5. Same as Table 4, except the superlattice has a rational wave number ratio. The parameters are $\alpha = 1$, $\delta = 1$, and $\kappa_2 = 3\kappa_1/2 = 3$.

θ	V_1	V_2	Analytical ε	Numerical ε
$\pi/16$	0.981	0.195	1.721	0.556
$\pi/8$	0.924	0.383	1.324	0.519
$3\pi/16$	0.831	0.556	1.152	0.505
$\pi/4$	0.707	0.707	1.077	0.510
$5\pi/16$	0.556	0.831	1.069	0.542
$3\pi/8$	0.383	0.924	1.128	0.601
$7\pi/16$	0.195	0.981	1.294	0.692

Table 6. Same as Table 4, except the superlattice has an irrational wave number ratio. The parameters are $\alpha = 1$, $\delta = 1$, and $\kappa_2 = \sqrt{2}\kappa_1 = \sqrt{2}$.

θ	V_1	V_2	Analytical ε	Numerical ε
$\pi/16$	0.981	0.195	1.721	0.642
$\pi/8$	0.924	0.383	1.333	0.511
$3\pi/16$	0.831	0.556	1.167	0.453
$\pi/4$	0.707	0.707	1.096	0.421
$5\pi/16$	0.556	0.831	1.093	0.410
$3\pi/8$	0.383	0.924	1.159	0.409
$7\pi/16$	0.195	0.981	1.340	0.394

for $\kappa_2/\kappa_1 = 3$ are shown in Tables 1 and 4, those for $\kappa_2/\kappa_1 = 3/2$ are shown in Tables 2 and 5, and those for $\kappa_2/\kappa_1 = \sqrt{2}$ are shown in Tables 3 and 6. Strictly speaking, our perturbative analysis does not apply to the numerical results in Tables 1, 4–6 because ε is too large. However, one can rescale the parameter V_0 to reduce the size of $\varepsilon_{\rm cr}$ so that the analysis leading to (45) is valid. From (41), we see that $k_i \propto \sqrt{V_0}$ and hence that $\varepsilon_{\rm cr} \propto 1/V_0$. We nevertheless use $V_0 = 1$ in Tables 4–6 to allow a more direct comparison with the results in Tables 1–3.

When ε is small, resonance regions arise from invariant tori of the form $(1/2)P_R^2 + (1/2)\delta R^2 + (1/4)\alpha R^4 = C_i = \text{constant}$, where $i \in \{1, 2\}$ denotes whether the resonance is respect to the primary or secondary lattice. Poincaré sections for

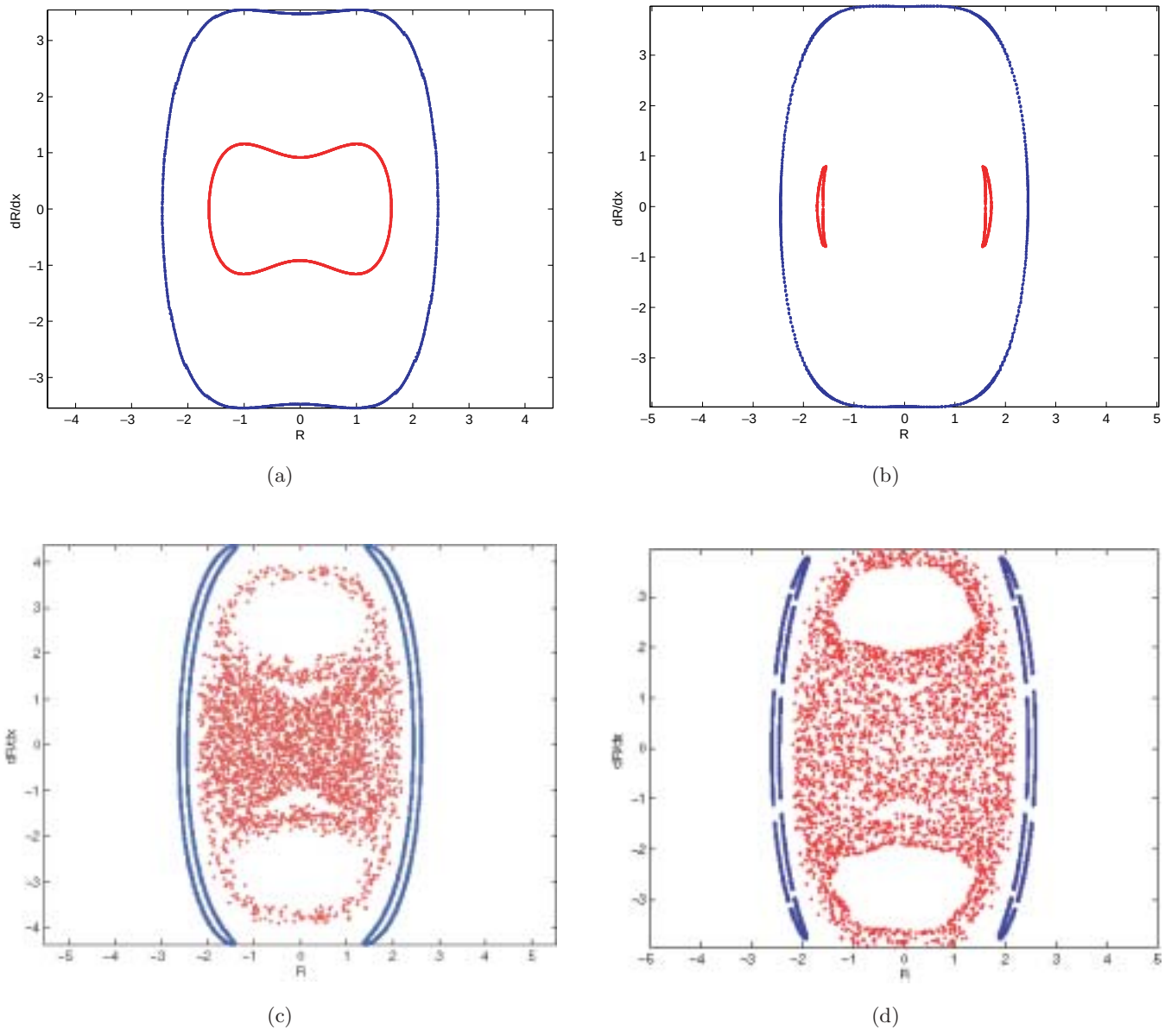

Fig. 1. Poincaré sections, strobed at $2m\pi/\kappa_1 = 2m\pi$ (for integer m), for Eq. (6) for an attractive condensate with a negative chemical potential. These plots, whose horizontal axis is R and whose vertical axis is $P_R = R' = dR/dx$, depict the case $\theta = \pi/4$, so that the primary and secondary lattices contribute equally. The initial conditions for the inner (red) and outer (blue) Poincaré sections are $(R, R') = (1.624, 0)$ and $(R, R') = (2.452, 0)$, respectively. (We use initial conditions with both positive and negative $R(0)$ in appropriate plots.) The lattice depths are (a) $\varepsilon = 0$, (b) $\varepsilon = 0.20$, (c) $\varepsilon = 0.41$, (d) $\varepsilon = 0.45$, and (e) $\varepsilon = 0.70$. Observe the onset of global chaos in the inner trajectory.

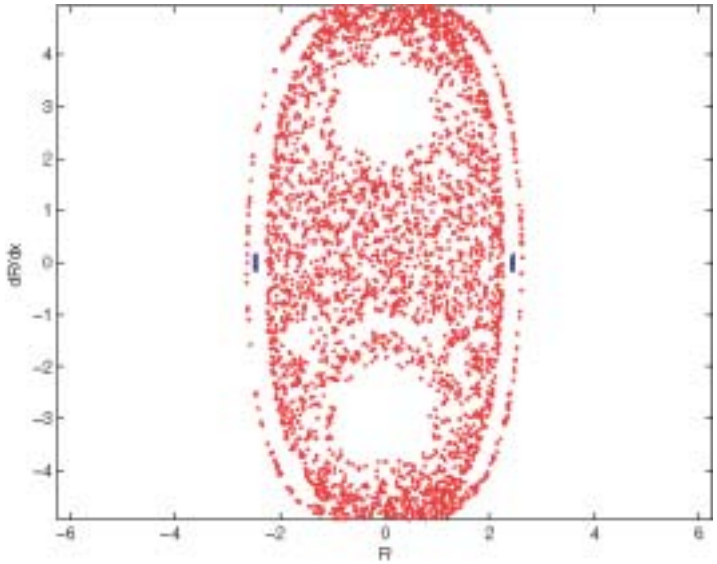

(e)

Fig. 1. (*Continued*)

an attractive BEC with a negative chemical potential and parameters $\kappa_1 = 1$, $\kappa_2 = 3\kappa_1 = 3$, $\theta = \pi/4$, and $\varepsilon = 0,\ 0.20,\ 0.41,\ 0.45,\ 0.70,$ are depicted in Fig. 1. (Numerical integration was performed using a Runge–Kutta integrator with step size 0.01.) The inner curves correspond to resonances with respect to the primary lattice harmonic. The outer curves correspond to resonances with respect to the secondary lattice harmonic. Initial conditions for the inner and outer curves were obtained by substituting $Y^{*(i)} = P_1^{(i)} \approx p_1^{(i)} = p^{(i)}$ and $q^{(i)} = 0$ for $i \in \{1, 2\}$ into (22) to determine $R(0)$ when $R'(0) = 0$. (The approximation of $P_1^{(i)}$ by $p_1^{(i)}$ is better for smaller ε and exact for $\varepsilon = 0$. We use initial conditions obtained from $\varepsilon = 0$ in our numerical simulations.) The spatial profiles $R = R(x)$ for $\varepsilon = 0.41$ and $\varepsilon = 0.45$ are shown in Figs. 2 and 3, respectively.

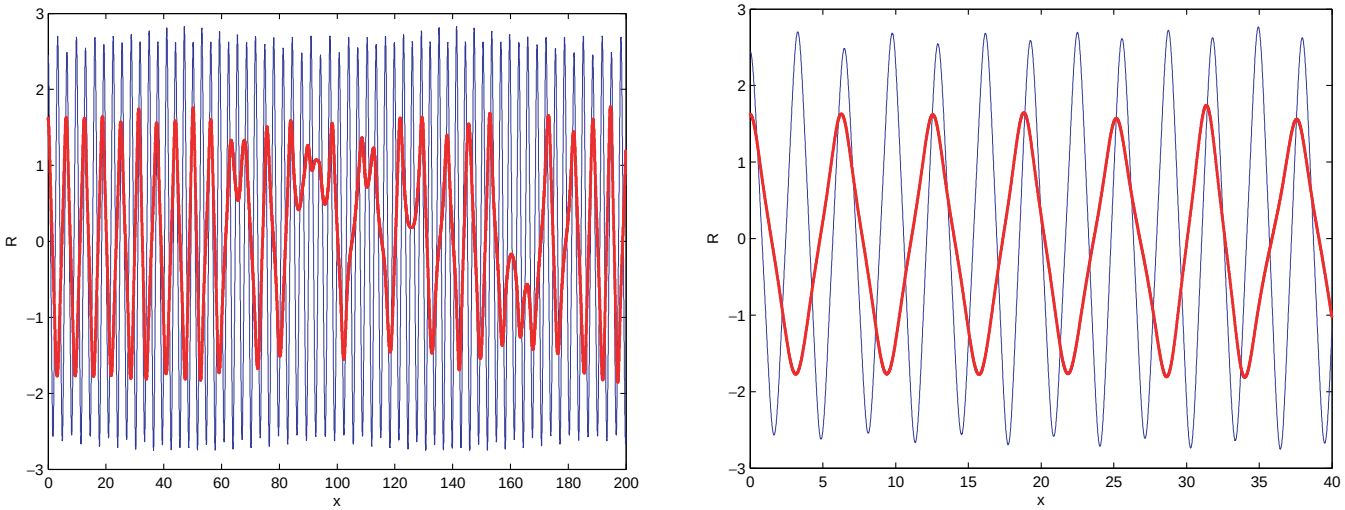

(a) (b)

Fig. 2. Spatial profiles $R = R(x)$ for an attractive condensate with a negative chemical potential. Trajectories are plotted at the same initial conditions as in Fig. 1. The parameters are $\kappa_1 = 1$, $\kappa_2 = 3$, $\theta = \pi/4$, and $\varepsilon = 0.41$. (a) Trajectories from $x = 0$ to $x = 200$. (b) Magnified view of trajectories from $x = 0$ to $x = 40$.

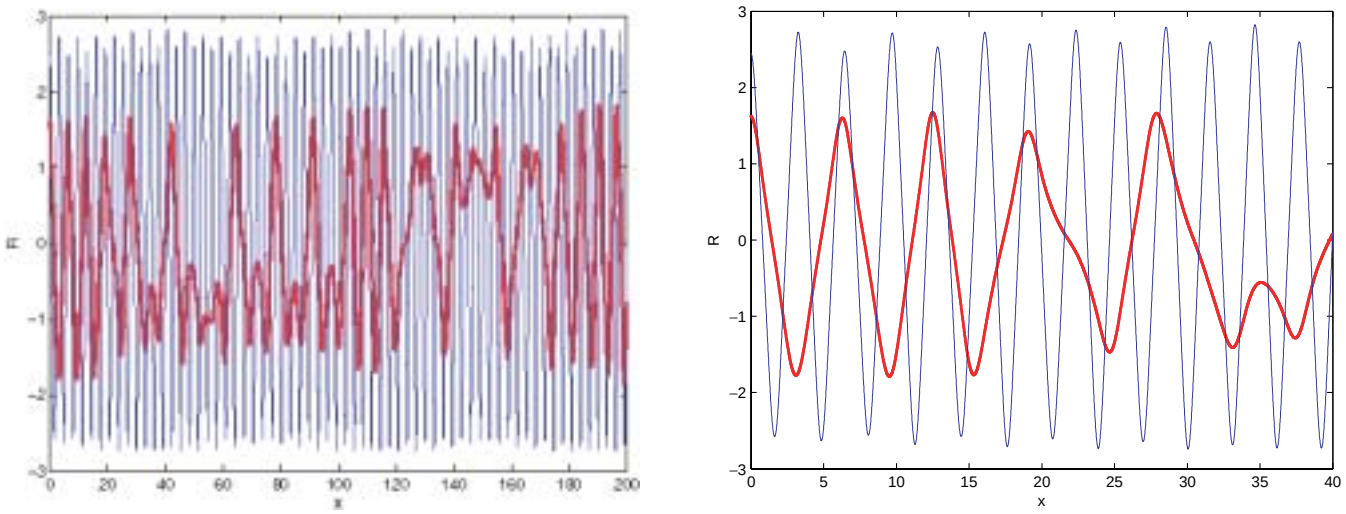

(a) (b)

Fig. 3. Spatial profiles $R = R(x)$ for an attractive condensate with a negative chemical potential. Trajectories are plotted at the same initial conditions as in Fig. 1. The parameters are $\kappa_1 = 1$, $\kappa_2 = 3$, $\theta = \pi/4$, and $\varepsilon = 0.45$. (a) Trajectories from $x = 0$ to $x = 200$. (b) Magnified view of trajectories from $x = 0$ to $x = 40$.

Poincaré sections for an attractive BEC with a positive chemical potential and parameters $\kappa_1 = 1$, $\kappa_2 = 3$, $\theta = \pi/4$, and $\varepsilon = 0$, 0.52, 0.83, 0.96, 1.15 are depicted in Fig. 4. The inner and outer curves are defined as above. The spatial profiles $R = R(x)$ for $\varepsilon = 0.83$ and $\varepsilon = 0.96$ are shown in Figs. 5 and 6, respectively. Initial conditions were determined just as for the case of negative chemical potentials.

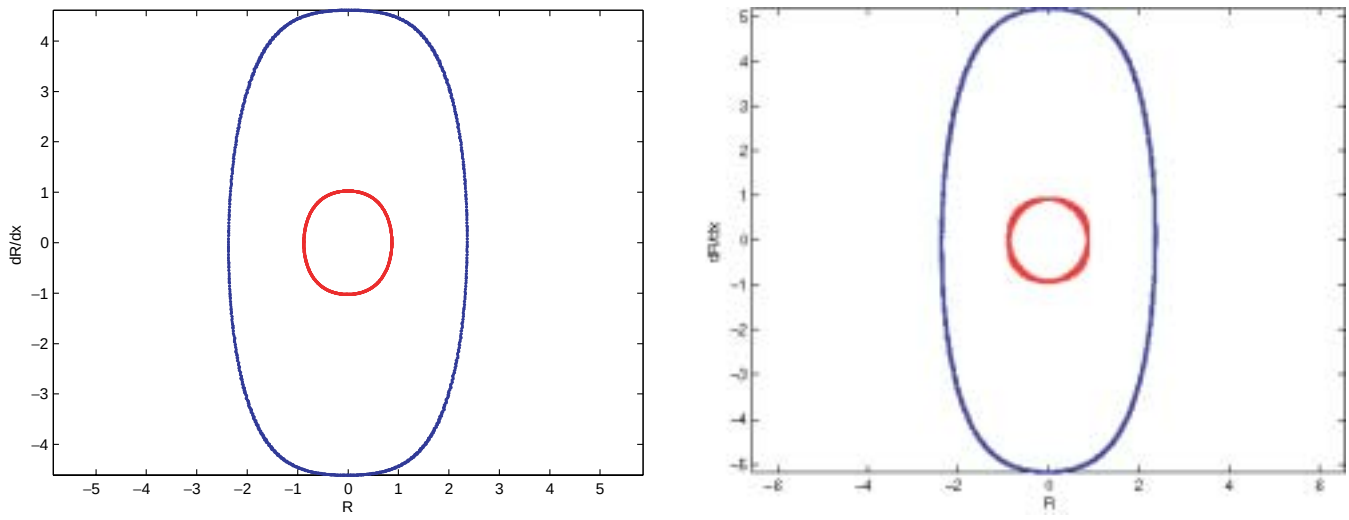

(a) (b)

Fig. 4. Poincaré sections, strobed at $2m\pi/\kappa_1 = 2m\pi$ (for integer m), for Eq. (6) for an attractive condensate with a positive chemical potential. These plots, with axes defined as in Fig. 1, depict the case $\theta = \pi/4$, so that the primary and secondary lattices contribute equally. The initial conditions for the inner (red) and outer (blue) Poincaré sections are $(R, R') = (0.873, 0)$ and $(R, R') = (2.366, 0)$, respectively. The lattice depths are (a) $\varepsilon = 0$, (b) $\varepsilon = 0.40$, (c) $\varepsilon = 0.83$, (d) $\varepsilon = 0.96$, and (e) $\varepsilon = 1.15$. Observe the onset of global chaos in the inner trajectory.

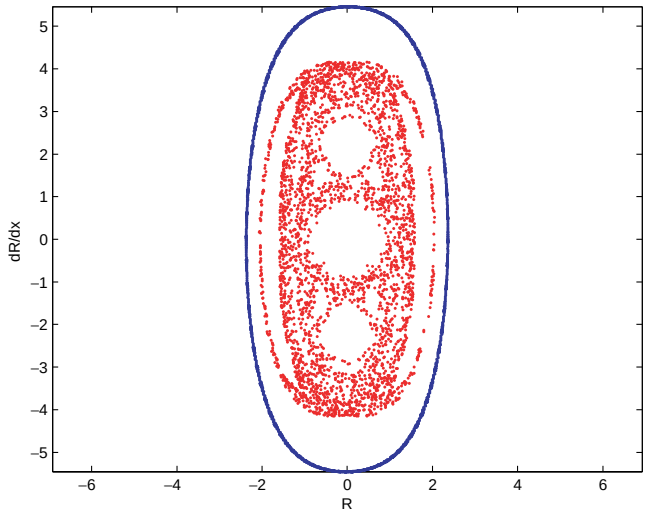

(c)

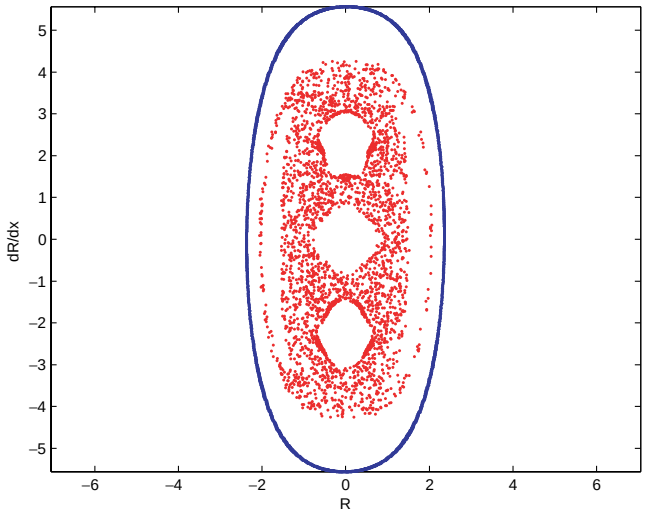

(d)

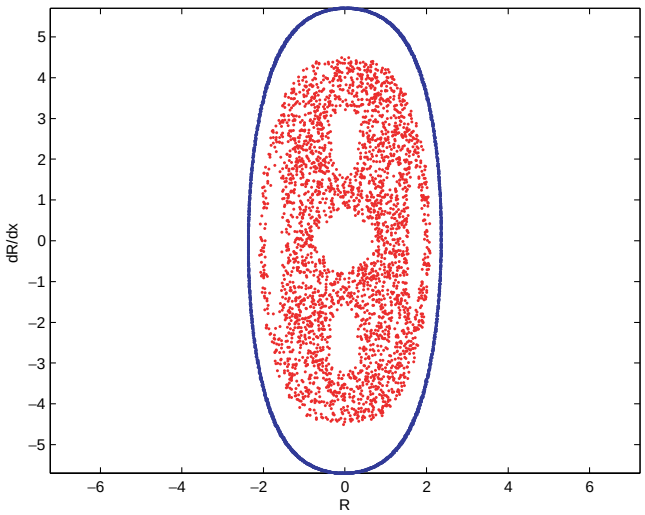

(e)

Fig. 4. (*Continued*)

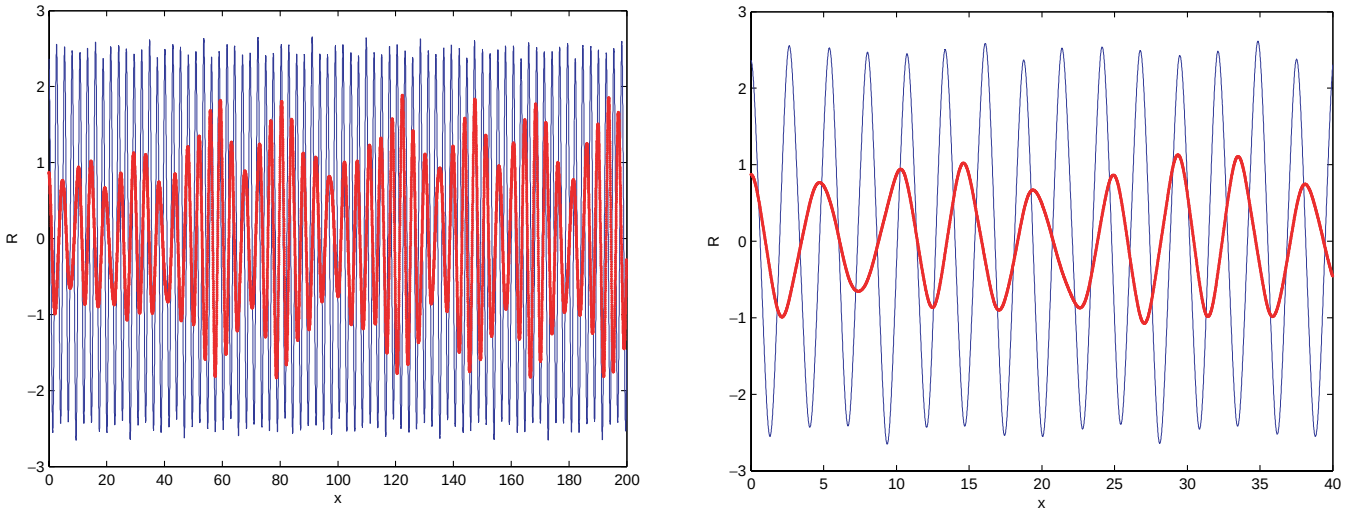

(a) (b)

Fig. 5. Spatial profiles $R = R(x)$ for an attractive condensate with a positive chemical potential. Trajectories are plotted at the same initial conditions as in Fig. 4. The parameters are $\kappa_1 = 1$, $\kappa_2 = 3$, $\theta = \pi/4$, and $\varepsilon = 0.83$. (a) Trajectories from $x = 0$ to $x = 200$. (b) Magnified view of trajectories from $x = 0$ to $x = 40$.

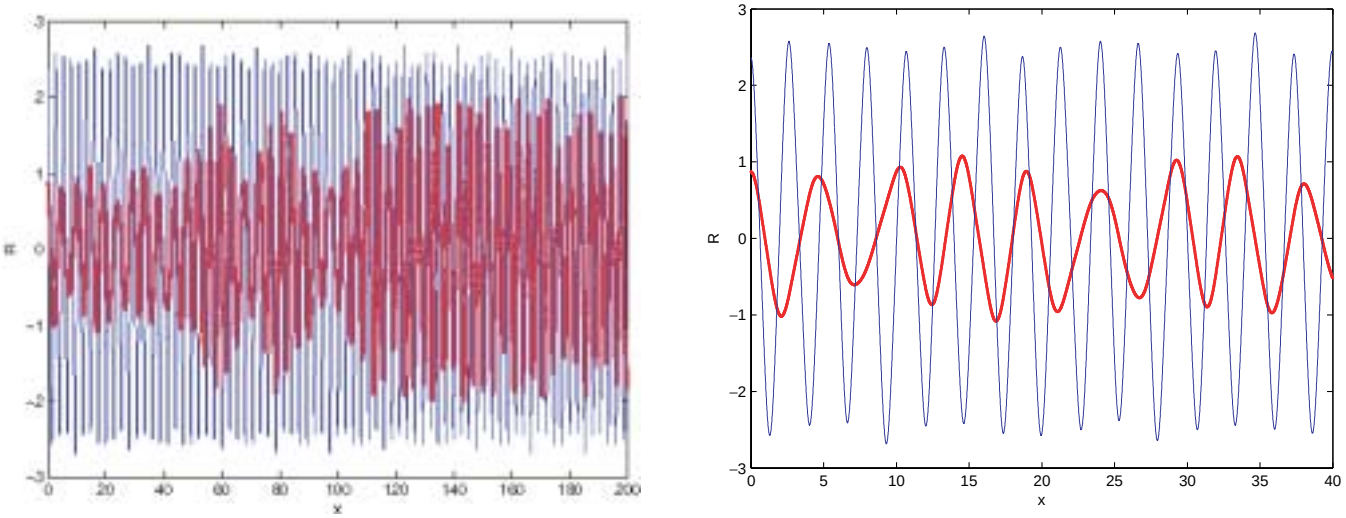

(a) (b)

Fig. 6. Spatial profiles $R = R(x)$ for an attractive condensate with a positive chemical potential. Trajectories are plotted at the same initial conditions as in Fig. 4. The parameters are $\kappa_1 = 1$, $\kappa_2 = 3$, $\theta = \pi/4$, and $\varepsilon = 0.96$. (a) Trajectories from $x = 0$ to $x = 200$. (b) Magnified view of trajectories from $x = 0$ to $x = 40$.

5. Conclusion

In this work, we derived analytically an upper bound for the critical lattice depth at which the spatial dynamics of BECs in superlattice potentials exhibits a transition from local to global chaos. This transition arises from overlap between spatial resonances with respect to individual lattice harmonics. We considered attractive BECs with both positive and negative chemical potentials and investigated the change in the derived estimate as the relative superlattice amplitudes from its two harmonics are adjusted. We also extracted the sizes of the associated resonance zones. To obtain our estimates, we examined coherent structure solutions of the Gross–Pitaevskii equation governing the mean-field dynamics of BECs and applied Chirikov's overlap criterion to the resulting parametrically

forced Duffing oscillator describing the BEC spatial dynamics. We supported our analytical work with numerical simulations.

Acknowledgments

We acknowledge support provided by a VIGRE grant awarded to the School of Mathematics at Georgia Tech. V. P. Chua also acknowledges support from a Georgia Tech PURA grant. We also thank Richard Rand for useful discussions concerning this project.

References

Anderson, B. P. & Kasevich, M. A. [1998] "Macroscopic quantum interference from atomic tunnel arrays," *Science* **282**, 1686–1689.

Anderson, M. H., Ensher, J. R., Matthews, M. R., Wieman, C. E. & Cornell, E. A. [1995] "Observation of Bose–Einstein condensation in a dilute atomic vapor," *Science* **269**, 198–201.

Baizakov, B. B., Konotop, V. V. & Salerno, M. [2002] "Regular spatial structures in arrays of Bose–Einstein condensates induced by modulational instability," *J. Phys. B*: *Atom. Molecul. Opt. Phys.* **35**, 5105–5119.

Band, Y. B., Towers, I. & Malomed, B. A. [2003] "Unified semiclassical approximation for Bose–Einstein condensates: Application to a BEC in an optical potential," *Phys. Rev. A* **67**, 023602.

Bronski, J. C., Carr, L. D., Carretero-González, R., Deconinck, B., Kutz, J. N. & Promislow, K. [2001a] "Stability of attractive Bose–Einstein condensates in a periodic potential," *Phys. Rev. E* **64**, 056615.

Bronski, J. C., Carr, L. D., Deconinck, B. & Kutz, J. N. [2001b] "Bose–Einstein condensates in standing waves: The cubic nonlinear Schrödinger equation with a periodic potential," *Phys. Rev. Lett.* **86**, 1402–1405.

Bronski, J. C., Carr, L. D., Deconinck, B., Kutz, J. N. & Promislow, K. [2001c] "Stability of repulsive Bose–Einstein condensates in a periodic potential," *Phys. Rev. E* **63**, 036612.

Brusch, L., Zimmermann, M. G., van Hecke, M., Bär, M. & Torcini, A. [2000] "Modulated amplitude waves and the transition from phase to defect chaos," *Phys. Rev. Lett.* **85**, 86–89.

Brusch, L., Torcini, A., van Hecke, M., Zimmermann, M. G. & Bär, M. [2001] "Modulated amplitude waves and defect formation in the one-dimensional complex Ginzburg–Landau equation," *Physica D* **160**, 127–148.

Burnett, K., Edwards, M. & Clark, C. W. [1999] "The theory of Bose–Einstein condensation of dilute gases," *Phys. Today* **52**, 37–42.

Cataliotti, F. S., Fallani, L., Ferlaino, F., Fort, C., Maddaloni, P. & Inguscio, M. [2003] "Superfluid current disruption in a chain of weakly coupled Bose–Einstein condensates," *New J. Phys.* **5**, 71.1–71.7.

Dalfovo, F., Giorgini, S., Pitaevskii, L. P. & Stringari, S. [1999] "Theory of Bose–Einstein condensation in trapped gases," *Rev. Mod. Phys.* **71**, 463–512.

Davis, K. B., Mewes, M.-O., Andrews, M. R., van Druten, N. J., Durfee, D. S., Kurn, D. M. & Ketterle, W. [1995] "Bose–Einstein condensation in a gas of sodium atoms," *Phys. Rev. Lett.* **75**, 3969–3973.

Donley, E. A., Claussen, N. R., Cornish, S. L., Roberts, J. L., Cornell, E. A. & Weiman, C. E. [2001] "Dynamics of collapsing and exploding Bose–Einstein condensates," *Nature* **412**, 295–299.

Eksioglu, Y., Vignolo, P. & Tosi, M. [2004] "Matter-wave interferometry in periodic and quasi-periodic arrays," *Opt. Commun.* **243**, 175–181.

Goldstein, H. [1980] *Classical Mechanics*, 2nd edition (Addison-Wesley Publishing Company, Reading, MA).

Greiner, M., Mandel, O., Esslinger, T., Hänsch, T. & Bloch, I. [2002] "Quantum phase transition from a superfluid to a Mott insulator in a gas of ultracold atoms," *Nature* **415**, 39–44.

Guckenheimer, J. & Holmes, P. [1983] *Nonlinear Oscillations, Dynamical Systems, and Bifurcations of Vector Fields*, Applied Mathematical Sciences, Vol. 42 (Springer-Verlag, NY).

Ketterle, W. [1999] "Experimental studies of Bose–Einstein condensates," *Phys. Today* **52**, 30–35.

Köhler, T. [2002] "Three-body problem in a dilute Bose–Einstein condensate," *Phys. Rev. Lett.* **89**, 210404.

Lawden, D. F. [1989] *Elliptic Functions and Applications*, Applied Mathematical Sciences, Vol. 80 (Springer-Verlag, NY).

Lichtenberg, A. J. & Lieberman, M. A. [1992] *Regular and Chaotic Dynamics*, 2nd edition, Applied Mathematical Sciences, Vol. 38 (Springer-Verlag, NY).

Louis, P. J. Y., Ostrovskaya, E. A. & Kivshar, Y. S. [2004] "Matter-wave dark solitons in optical lattices," *J. Opt. B*: *Quant. Semiclass. Opt.* **6**, S309–S317.

Louis, P. J. Y., Ostrovskaya, E. A. & Kivshar, Y. S. [2005] "Dispersion control for matter waves and gap solitons in optical superlattices," *Phys. Rev. A* **71**, 023612.

Morsch, O., Müller, J. H., Christiani, M., Ciampini, D. & Arimondo, E. [2001] "Bloch oscillations and mean-field effects of Bose–Einstein condensates in 1D optical lattices," *Phys. Rev. Lett.* **87**, 140402.

Orzel, C., Tuchman, A. K., Fenselau, M. L., Yasuda, M. & Kasevich, M. A. [2001] "Squeezed states in a Bose–Einstein condensate," *Science* **291**, 2386–2389.

Pedri, P., Pitaevskii, L., Stringari, S., Fort, C., Burger, S., Cataliotii, F. S., Maddaloni, P., Minardi, F. & Inguscio, M. [2001] "Expansion of a coherent

array of Bose–Einstein condensates," *Phys. Rev. Lett.* **87**, 220401.

Peil, S., Porto, J. V., Laburthe Tolra, B., Obrecht, J. M., King, B. E., Subbotin, M., Rolston, S. L. & Phillips, W. D. [2003] "Patterned loading of a Bose–Einstein condensate into an optical lattice," *Phys. Rev. A* **67**, 051603(R).

Pethick, C. J. & Smith, H. [2002] *Bose–Einstein Condensation in Dilute Gases* (Cambridge University Press, Cambridge, UK).

Porter, M. A. & Cvitanović, P. [2004a] "Modulated amplitude waves in Bose–Einstein condensates," *Phys. Rev. E*, 047201.

Porter, M. A. & Cvitanović, P. [2004b] "A perturbative analysis of modulated amplitude waves in Bose–Einstein condensates," *Chaos* **14**, 739–755.

Porter, M. A. & Kevrekidis, P. G. [2005] "Bose–Einstein condensates in superlattices," *Siam. J. App. Dyn. Syst.* **4**, 783–807.

Porter, M. A., Kevrekidis, P. G., Carretero González, R. & Frantzeskakis, D. J. [2006] "Dynamics and manipulation of matter-wave solitons in optical superlattices," *Phys. Lett. A* **352**, 210–215.

Porto, J. V., Rolston, S., Laburthe Tolra, B., Williams, C. J. & Phillips, W. D. [2003] "Quantum information with neutral atoms as qubits," *Philo. Trans.: Math. Phys. Engin. Sci.* **361**, 1417–1427.

Rand, R. H. [1994] *Topics in Nonlinear Dynamics with Computer Algebra*, Computation in Education: Mathematics, Science and Engineering, Vol. 1 (Gordon and Breach Science Publishers, USA).

Rey, A. M., Hu, B., Calzetta, E., Roura, A. & Clark, C. [2004] "Nonequilibrium dynamics of optical lattice-loaded BEC atoms: Beyond HFB approximation," *Phys. Rev. A* **69**, 033610.

Salasnich, L., Parola, A. & Reatto, L. [2002] "Periodic quantum tunnelling and parametric resonance with cigar-shaped Bose–Einstein condensates," *J. Phys. B: Atom. Molec. Opt. Phys.* **35**, 3205–3216.

Smerzi, A., Trombettoni, A., Kevrekidis, P. G. & Bishop, A. R. [2002] "Dynamical superfluid-insulator transition in a chain of weakly coupled Bose–Einstein condensates," *Phys. Rev. Lett.* **89**, 170402.

van Noort, M., Porter, M. A., Yi, Y. & Chow, S.-N. [2004] "Quasiperiodic and chaotic dynamics in Bose–Einstein condensates in periodic lattices and superlattices," e-print: arXiv:math.DS/0405112.

Vollbrecht, K. G. H., Solano, E. & Cirac, J. L. [2004] "Ensemble quantum computation with atoms in periodic potentials," *Phys. Rev. Lett.* **93**, 220502.

Zounes, R. S. & Rand, R. H. [2001] "Global behavior of a nonlinear quasiperiodic Mathieu equation," in *Proc. DETC2001*, 2001 ASME Design Engineering Technical Conf., No. VIB-21595, pp. 1–11.

Zounes, R. S. & Rand, R. H. [2002a] "Global behavior of a nonlinear quasiperiodic Mathieu equation," *Nonlin. Dyn.* **27**, 87–105.

Zounes, R. S. & Rand, R. H. [2002b] "Subharmonic resonance in the non-linear Mathieu equation," *Int. J. Non-Lin. Mech.* **37**, 43–73.